Curaxins and G-Quadruplex DNA Oligomers

Subjects: Cell Biology

Contributor: Ramon Eritja

Curaxins and especially the second-generation derivative curaxin CBL0137 have important antitumor activities in multiple cancers such as glioblastoma, melanoma and others. Although most of the authors suggest that their mechanism of action comes from the activation of p53 and inactivation of NF-kB by targeting FACT, there is evidence supporting the involvement of DNA binding in their antitumor activity. In this work, the DNA binding properties of curaxin CBL0137 with model quadruplex DNA oligomers were studied by 1H NMR, CD, fluorescence and molecular modeling. We provided molecular details of the interaction of curaxin with two G-quadruplex structures, the single repeat of human telomere d(TTAGGGT)4 and the c-myc promoter Pu22 sequence.

Keywords: curaxin ; NMR spectroscopy ; circular dichroism ; G-quadruplex ; molecular modeling ; DNA interactions ; c-myc

1. Introduction

Curaxins are a small group of substances endowed with anticancer activity [1]. They were identified in a search for non-genotoxic antiproliferative compounds, simultaneously acting on two tumor targets. The first hits found were quinacrine and other antimalarials, but SAR studies led rapidly to more active compounds, represented by curaxins, a class of substituted carbazoles with electron-withdrawing groups at positions 3 and 6, and an aminoalkyl chain at the nitrogen 9. Curaxins are able to activate the tumor suppressing protein p53 and to suppress the anti-apoptotic nuclear factor NF-κB [2][3]. Importantly, curaxins were found to be more toxic to tumor than to normal cells. Among curaxins, CBL0137 (Figure 1), appeared the most suitable for further development, on the basis of its metabolic stability, solubility and activity in vivo. CBL0137 suppressed tumor growth in xenograft models of colon (DLD-1), renal cell carcinoma (Caki-1) [3], medulloblastoma [4], small-cell lung cancer [5][6], melanoma (Mel-7) and transplanted surgical samples from patients with pancreatic ductal adenocarcinoma [7].

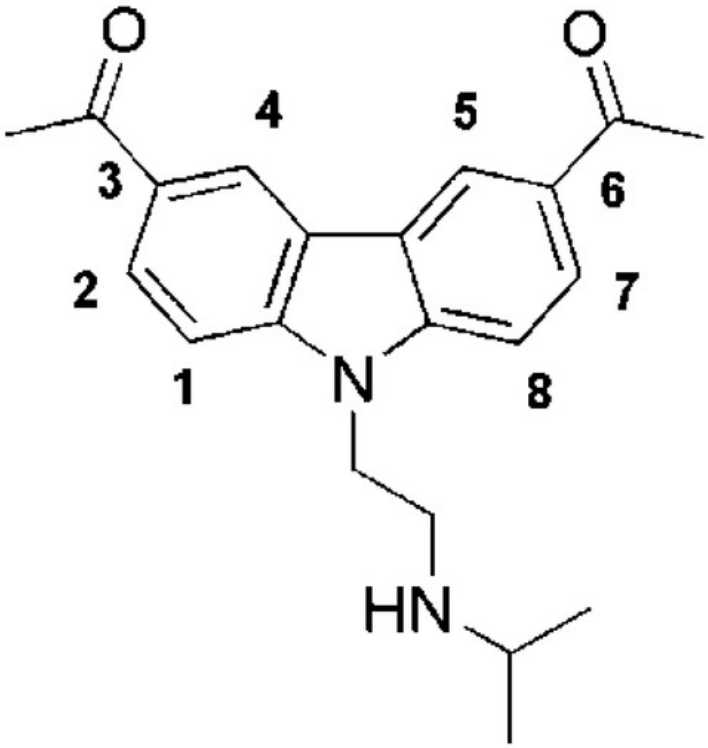

Figure 1. Structure of curaxin CBL0137.

CBL0137 was also found to be active in mixed-lineage leukemia [8] and against cancer stem cells and to potentiate efficacy of gemcitabine in pancreatic cancer [9].

At present, CBL0137 is under phase I clinical trials in patients with hematological malignancies and solid tumors [10].

The cytotoxicity of curaxins, which are associated with the absence of DNA damage, stimulated studies directed to unveil their mechanism of action. Eukaryotic DNA is packed into chromatin, which is a highly ordered complex of DNA and histone proteins. Its basic unit, the nucleosome, consists of an octamer of histones, known as the histone or nucleosome core, which is bound to a 147 base pairs of DNA fragment.

Recent studies suggested that CBL0137 interacts with DNA by modifying the shape of the DNA helix, thus increasing the interbase-pair distance. As a consequence, DNA unwinding and detachment from the histone octamer occur, eventually leading to nucleosome disassembly both in vitro and in cells. The destabilization of the nucleosomes induces the intervention of a histone chaperone, FACT (Facilitates Chromatin Transcription), which binds tightly to chromatin (c-trapping) [2][11][12]. This results in activating phosphorylation of p53 by FACT-associated CK2 and reducing NF-kB–dependent transcription, because of depletion of soluble FACT. Recently, it was reported that such effects are associated with the induction of the interferon response to epigenetic derepression of the cellular “repeatome” [13].

Kantidze et al. [14] found that CBL0137 alters DNA topology leading to the inability of the transcriptional repressor CTCF to bind efficiently to its cognate DNA sites. This effect on CTCF binding results in partial disruption of chromatin loops and in large-scale perturbations in the 3D genome organization.

More recently, Lu et al. [15] tried to clarify how curaxins alter the genomic DNA structure and affect the DNA binding property of key proteins, such as CTCF and FACT. They found that CBL0137 strongly and persistently binds to dsDNA, inducing a huge barrier for DNA unzipping during replication and transcription, thus causing the distinct binding response of CTCF and FACT on DNA.

Further investigations revealed that several pathways, such as inhibition of the self-renewal of cancer stem cells/tumor-initiating cells through NOTCH1 activation and downregulation of heat shock factor 1 (HSF1), thereby increasing tumor cell apoptosis, are involved in the process [5][14][16]. Moreover, CBL037 highly suppresses the expression of c-MYC family genes. Sergeev et al. [17] reported that this curaxin significantly inhibits in vitro DNA methylation by eukaryotic DNA methyltransferase Dnmt3a at low micromolar concentrations. These effects are attributed to the intercalation of CBL0137 into DNA [3][11], although there is no direct evidence for this type of interaction. The change of topology of DNA by binding with CBL0137 was deduced from CD experiments [11], whereas molecular modeling studies showed a possible protruding of the side chains of the carbazole nucleus into the major groove of DNA, with the carbazole *N*-side chain filling the minor groove [11].

The above reported effects, including inhibition of c-MYC expression, DNA methyltransferase inhibition, and chromatin remodelling, would be consistent with DNA G-quadruplex binding [18][19].

G-quadruplexes are non-canonical nucleic acids secondary structures that may form in G-rich sequences under physiological conditions. Their structural building block is the G-quartet, a planar array of four guanines paired through Hoogsteen bonds. G-quadruplexes play a role in several key cellular processes, including gene transcription, chromatin epigenetics and DNA recombination. G-quadruplex DNA is found in key regulatory regions of the cell such as promoters of proto-oncogenes (*c-myc*, *bcl-2* and *c-Kit*) [20]. Stabilization of the folded G-quadruplexes due to ligand interactions is proposed to inhibit the binding of transcription factors, leading to downstream silencing of oncogene expression [21][22][23]. Notably, also human telomeric sequences are able to form G-quadruplex structures that are not recognized by telomerase, an enzyme involved in telomere elongation [24].

The planar structure with an aminoalkyl side chain of CBL0137, similar to other non-DNA-damaging G-quadruplex ligands [23], supports the hypothesis that G-quadruplex interaction can have a role in the curaxin activity; however, so far, no evidence has been given for such an interaction.

To confirm our hypothesis, we undertook an investigation of the binding of CBL0137 to G-quadruplex DNA structures of telomeres and promoter oncogenes by exploiting fluorescence spectroscopy, CD, NMR and molecular modelling. We used as models the single repeat sequence of human telomere, $d(TTAGGGT)_4$, and the G to T mutated Pu22 sequence (Pu22T14T23) of the *c-myc* oncogene, which is overexpressed in a wide range of human tumors.

To further investigate the possible intercalation mode of curaxin into the double helix DNA, as previously reported by some authors (References [3][11]), the study was extended to the self-complementary double helix oligomers d(CGTACG)$_2$ and d(AAGAATTCTT)$_2$ as models for CG and AT-rich sequences, respectively.

Our work provides a novel insight into the DNA-binding properties of CBL0137 that may be relevant in the important anticancer activity of curaxines.

2. Interaction of Curaxin with Telomere d(TTAGGGT)$_4$ Quadruplex

The imino proton region of the ^{1}H NMR spectrum of d(TTAGGGT)$_4$ showed three signals between 10 and 12 ppm that are indicative of the formation of a single G-quadruplex species with three G-quartet planes. As curaxin was added to the d(TTAGGGT)$_4$ solution, the NH imino protons moved upfield and G4 and G6 signals became broad even at low ratio R = [curaxin]/[DNA] = 0.25/0.75. At R = 2.0 the imino proton of G4 remained very broad, while the G6 became sharp again. This behavior can be explained by the binding of curaxin to G4 and G6 tetrads, with an intermediate exchange between free and bound state at the level of G4. The greatest variation of chemical shift is observed for G6 signal (Δδ = −0.55 ppm) (Figure 2).

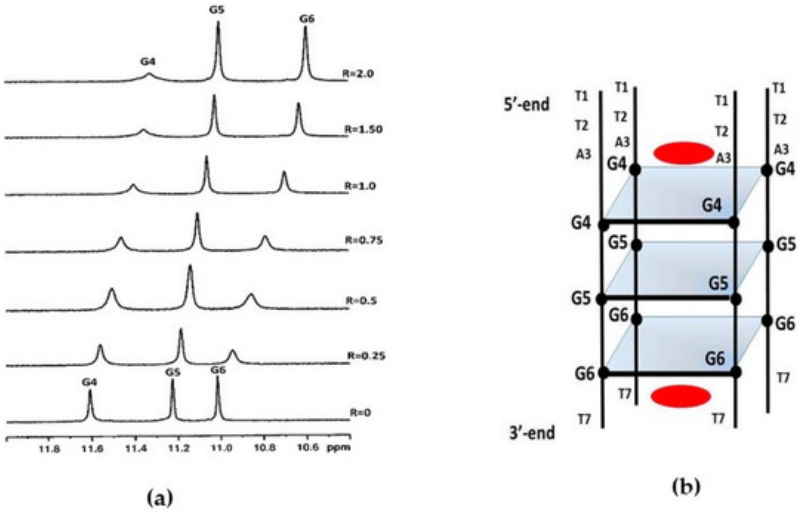

Figure 2. (**a**) Imino proton region of the 1D NMR titration spectra of d(TTAGGGT)$_4$ with curaxin at 25 °C in H_2O/D_2O (9:1), 25 mM KH_2PO_4, 150 mM KCl and 1 mM EDTA, pH 6.7, at different R = [drug]/[DNA] ratios; (**b**) schematic representation of d(TTAGGGT)$_4$/curaxin (in red) complex.

In order to better define the geometry of the complex, a series of 2D NMR experiments were performed. NOESY and TOCSY experiments allowed us to identify the curaxin (Table S1) and d(TTAGGGT)$_4$ protons in the complex (Table S2). Despite of the overlapping of some of curaxin and oligonucleotide signals, several intermolecular NOE interactions were detected. The contacts involved both aromatic and side chain protons of the curaxin with aromatic and ribose protons of d(TTAGGGT)$_4$ at A3G4 and G6T7 sites (Table 1 and Figure 3).

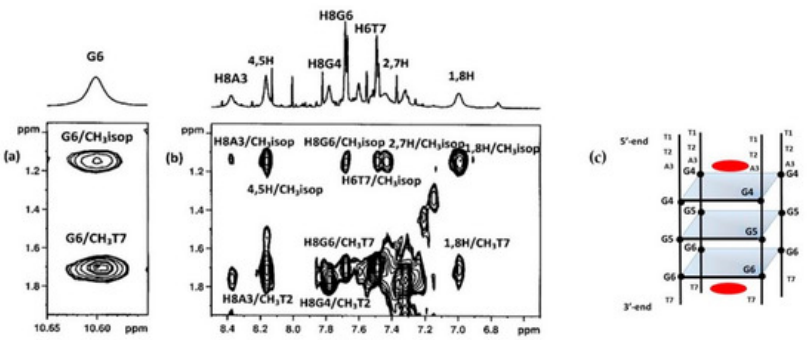

Figure 3. Selected region of the 2D NOESY spectrum of d(TTAGGGT)$_4$/curaxin complex. (**a**) G6 imino proton displays intermolecular NOEs between CH_3T7 and CH_3(isopropyl) of curaxin; (**b**) A3, G6 and T7 aromatic protons and methyl groups of T2 and T7 of T2AG3T display intermolecular NOEs with CH_3 (isopropyl) and aromatic protons of curaxin; (**c**) schematic representation of d(TTAGGGT)$_4$/curaxin (in red) complex.

Table 1. Intermolecular NOE and distances from modelling in the curaxin-d(TTAGGGT)$_4$ [a] complexes.

ApG Binding Site		
NOE		d (Å) [b]
Curaxin	d(TTAGGGT)$_4$	
1,8-H	A3H1′	4.60
2,7-H	A3H8	4.26
4,5-H	G4H1′	5.88
CH_3 iso	A3H8	3.20
	GpT Binding Site	
1,8-H	G6H8	5.45
1,8-H	G6H1	4.36
1,8-H	T7Me	4.74
1,8-H	T7H1	3.13
4,5-H	G6H1	3.55
CH_3 iso	G6H8	2.30
CH_3 iso	G6H1	4.91
CH_3 iso	T7H6	4.84
CH_3 iso	G5H1′	5.91

[a] Acquired at 25 °C in H_2O-D_2O (90:10 *v*/*v*), 25 mM K-phosphate buffer, 150 mM KCl and 1 mM EDTA, at pH 6.7. [b] Distances obtained by molecular modelling of the complex.

The NMR studies were complemented by a molecular docking simulation, followed by molecular dynamics (MD) optimization. Curaxin was docked at both A3G4 and G6T7 sites (Figure 4A). At the A3G4 binding site the ligand adopts a quite centre-symmetrical location, allowing the formation of π-π stacking interactions with all the bases of the upper A3 and lower G4 tetrads. In this site the complex is stabilized by a hydrogen bond between the charged quaternary nitrogen group of curaxin and N_7A3, at a distance of 2.44 Å. One of the two benzene rings of curaxin lies above the K^+ ion, resulting in a strong cation-π interaction (4.90 Å). The interaction pattern is completed by two other cation-π interactions formed between the quaternary nitrogen of the ligand and the aromatic component of the A3 and G4 bases (Figure 4B).

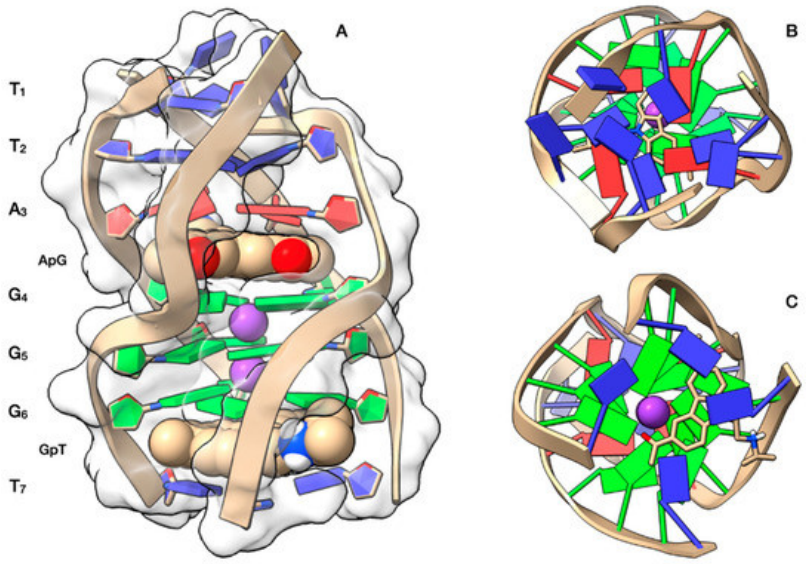

Figure 4. Graphical representations of the curaxin-d(TTAGGGT)$_4$ complexes at the ApG and GpT intercalation sites, obtained by Molecular Docking and optimized by Molecular Dynamics (MD). (**A**) Side view of the ghostly white solvent accessible surface (SAS) of the d(TTAGGGT)$_4$ quadruplex. The nucleotides are represented in stick and filled rings: adenine in red, guanine in green and thymine in blue. The ligand is represented as van der Waals (vdW) spheres and colored following the CPK code. The optimized conformations of the ligand are represented in (**B**) for the complex at ApG and in (**C**) for the complex at GpT. Potassium ions are represented by their vdW spheres (K^+ in purple), while the ligand is

depicted in stick and colored following the CPK code. The nucleotides are represented as filled plates: adenine in red, guanine in green and thymine in blue.

Otherwise, at the G6T7 site the ligand does not adopt a center-symmetrical stacking interaction but it is rather shifted towards one half of the G6 tetrad (Figure 4C). In this orientation, the ligand gives π-π stacking interactions with G6 and T7 and is stabilized by an attractive charge interaction between OP_2G6 and the charged quaternary nitrogen group of the ligand. The quaternary nitrogen is also involved in a cation-π interaction with the aromatic component of T7.

The best docked conformations of the complexes at the ApG and GpT intercalation sites are in good agreement with the reported NOE contacts (Table 1).

3. Interaction of Curaxin with Pu22T14T23 G-Quadruplex

An important and generalized line broadening of the guanine NH imino protons was observed upon the titration of Pu22T14T23 with curaxin, even at low ratio R = 0.25/1.0. This can be due to a strong interaction of the curaxin with the nucleotide, producing an intermediate exchange process between free and bound state on the NMR timescale. In particular, the NH signals belonging to the tetrad G9-G13-G18-G22 disappeared almost completely. At a ratio R > 1.0, the NH signals sharpened and for R = 2.0 only one set of resonance was present (Figure 5). By increasing the R value until a ratio of 4, the spectrum did not change significantly. All the signals moved upfield, but the most relevant chemical shift variation was observed for G7, G11 and G16 residues at 5′-end, and for G22, G18 and G13 at 3′-end. These findings indicate that a single conformation of the complex occurs in solution and suggest that the binding sites are at the level of the external tetrads.

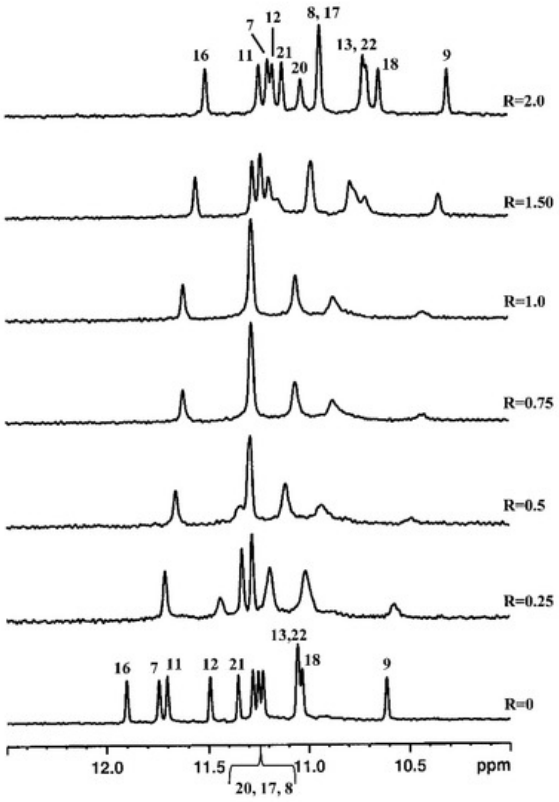

Figure 5. Imino proton region of the 1D NMR titration spectra of Pu22T14T23 with curaxin at 25 °C in H_2O/D_2O (9:1), 25 mM KH_2PO_4 and 70 mM KCl at pH 6.9, at different R = [drug]/[DNA] ratios.

The proton assignment and the inter-residue NOE connectivities characterizing the three tetrads in the complex are described in the Experimental section and the values are reported in Tables S3 and S4.

Many NOE interactions between curaxin and the nucleotide were revealed in the NOESY spectra (Table 2, Figure 6 and Figure S1). A large portion of the curaxin molecule, going from H1 and H2 to H7 and H8, including the side chain at N_9, has contacts with the aromatic protons of the guanines G7, G11 and G20 at 5′-end. At the same terminal, the CH_3CO groups of curaxin show strong interactions with the imino H1 protons of the guanines of the above tetrad.

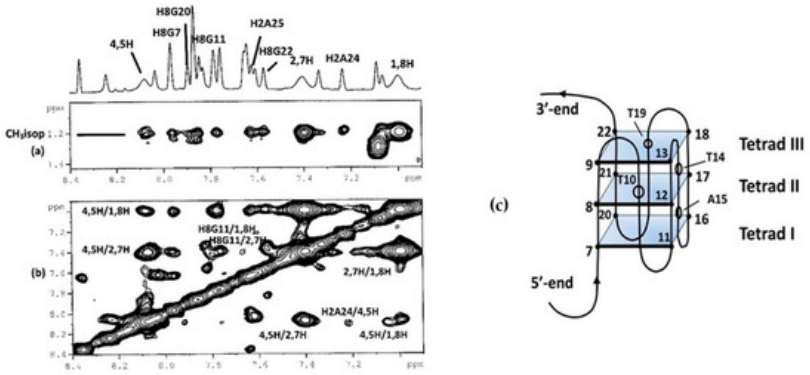

Figure 6. Selected region of the 2D NOESY spectrum of Pu22T14T23/curaxin complex. (**a**) Some aromatic protons of Pu22T14T23 display intermolecular NOEs with CH_3(isopropyl) of curaxin; (**b**) some aromatic protons of Pu22T14T23 display intermolecular NOEs with aromatic protons of curaxin and (**c**) schematic representation of Pu22-T14 T23 oligomer G-quadruplex.

Table 2. Intermolecular NOEs and distances from modelling in the curaxin-Pu22T14T23 [a] complex.

3′-Binding Site NOE		**d (Å) [b]**
Curaxin	**Pu22T14T23**	
4,5-H	**G18H1**	**5.69**
4,5-H	**A24H2**	**6.60**
CH_3CO	**G13H1**	**5.38**
CH_3CO	**G22H1**	**4.68**
$CH_{3\ iso}$	**A24H2**	**6.21 [c]**
$CH_{3\ iso}$	**A25H2**	**4.25**
CH_3CO	**G18H1**	**2.26**
5′-Binding Site NOE		
1,8-H	**G7H1′**	**7.39 [c]**
2,7-H	**G11H8**	**3.97**
1,8-H	**G11H8**	**5.34**
$CH_{3\ iso}$	**G20H8**	**2.75**
$CH_{3\ iso}$	**T4H1′**	**6.22 [c]**
CH_3CO	**G7H1**	**4.90**
CH_3CO	**G11H1**	**3.45**

[a] Acquired at 25 °C in H_2O-D_2O (90:10 *v*/*v*), 25 mM KH_2PO_4, 70 mM KCl, pH 6.9. [b] Distances obtained by molecular modelling of the complex. [c] The long distance is explained with the mobility of the ligand and the tails of the nucleotide.

The 3′-end terminal appears more compact. H4,5 and CH_3CO groups present strong NOE interactions with the imino protons H1 of G18 and H1 of G22 and/or G13, respectively. In addition, both aromatic and methyl protons show significant contacts with the tail of the flanking chain A24 and A25.

These results indicate that curaxin binds the Pu22T14T23 quadruplex over the two external tetrads. The location at 3′-end appears more stable, while the interaction at 5′-end terminal seems to be characterized by a higher mobility of the ligand. This relative mobility is also suggested by the finding of additional weak NOE interactions involving the ribose H1′ proton of G7 and T4 units with H1,8 and the side chain of the ligand.

The three-dimensional models for the curaxin-Pu22T14T23 complexes were obtained by performing molecular docking experiments, followed by a Molecular Dynamics (MD) optimization of the resulting complexes (Figure 7). In both 3′-end and 5′-end positions, the curaxin molecule is arranged along the main groove of Pu22.

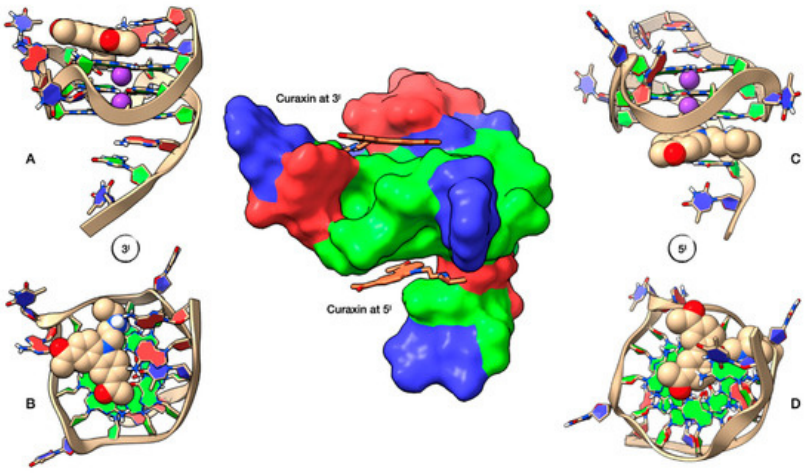

Figure 7. Representation of the Pu22T14T23 complexes with curaxin at 5'-end and 3'-end, obtained by Molecular Docking and optimized by Molecular Dynamics (MD). At the center of the figure Pu22T14T23, represented by its solvent accessible surface (SAS), color-coded by the underlying nucleotide (adenine in red, guanine in green and thymine in blue) and complexed with curaxin (represented in stick) at both 3'-end and 5'-end. On the left, lateral (**A**) and top (**B**) representation of the ligand conformation at the 3'-end, while on the right we can see the lateral (**C**) and bottom (**D**) representation of curaxin at the 5'-end. Ligand and potassium ions are represented by their van der Waals spheres (ligand colored in CPK, K^+ in purple), while the nucleotide units of Pu22T14T23 are represented as filled rings: adenine in red, guanine in green and thymine in blue.

At 3'-end, the ligand is positioned towards the center of the tetrad and is stabilized by a π–π interaction involving G13 and one of the two benzene rings. The side chain faces A25, forming two hydrogen bonds between the quaternary nitrogen protons and N_1A25, with distances of 2.69 Å and 2.57 Å. This explains the downfield shift of A25 H2 (Δδ + 0.21 ppm), which has lost the shielding by the aromatic system of the guanine G22. No particular interactions involving the two CH_3CO residues are observed. (Figure 7A,B).

At 5'-end, curaxin is stabilized by an extensive network of π–π interactions involving the underlying 5'-end G-tetrad, with the tricyclic moiety located near the center of the tetrad (Figure 7C,D). The aromatic system interacts with the π systems of G5, G7, G11 and G16. The complex is held in place by two cation-π interaction. The first between the potassium ion and the pyrrole moiety (4.93 Å) and the second between the quaternary nitrogen of the side chain and the aromatic system of G7. The system is further stabilized by a hydrogen bond between one carbonyl group (CH_3CO) and G7 H1 (3.06 Å), and by a bidentate hydrogen bond between the quaternary nitrogen of the curaxin and G5 N_7 (2.82 Å) and A6 N1 (2.70 Å).

The best conformations of the complexes at 5'-end and 3'-end are in agreement with the reported NOE contacts (Table 2).

References

1. Di Bussolo, V.; Minutolo, F. Curaxins: A New Family of Non-genotoxic Multitargeted Anticancer Agents. ChemMedChem 2011, 6, 2133–2136.
2. Gurova, K.V.; Hill, J.E.; Guo, C.; Prokvolit, A.; Burdelya, L.G.; Samoylova, E.; Khodyakova, A.V.; Ganapathi, R.; Ganapathi, M.; Tararova, N.D.; et al. Small molecules that reactivate p53 in renal cell carcinoma reveal a NF-κB-dependent mechanism of p53 suppression in tumors. Proc. Natl. Acad. Sci. USA 2005, 102, 17448–17453.
3. Gasparian, A.V.; Burkhart, C.A.; Purmal, A.A.; Brodsky, L.; Pal, M.; Saranadasa, M.; Bosykh, D.A.; Commane, M.; Guryanova, O.A.; Pal, S.; et al. Curaxins: Anticancer Compounds That Simultaneously Suppress NF-κB and Activate p53 by Targeting FACT. Sci. Transl. Med. 2011, 3, 95ra74.
4. Wang, J.; Sui, Y.; Li, Q.; Zhao, Y.; Dong, X.; Yang, J.; Liang, Z.; Han, Y.; Tang, Y. Effective inhibition of MYC-amplified group 3 medulloblastoma by FACT-targeted curaxin drug CBL0137. Cell Death Dis. 2020, 11, 1029.
5. De, S.; Lindner, D.J.; Coleman, C.J.; Wildey, G.; Dowlati, A.; Stark, G.R. The FACT inhibitor CBL0137 Synergizes with Cisplatin in Small-Cell Lung Cancer by Increasing NOTCH1 Expression and Targeting Tumor-Initiating Cells. Cancer Res. 2018, 78, 2396–2406.

6. Lindner, D.J.; Wildey, G.; Parker, Y.; Dowlati, A.; Stark, G.R.; De, S. CBL0137 increases the targeting efficacy of Rovalpituzumab tesirine against tumour-initiating cells in small cell lung cancer. Br. J. Cancer 2021, 124, 893–895.
7. Jin, M.Z.; Xia, B.R.; Xu, Y.; Jin, W.L. Curaxin CBL0137 Exerts Anticancer Activity via Diverse Mechanisms. Front. Oncol. 2018, 8, 598.
8. Somers, K.; Kosciolek, A.; Bongers, A.; El-Ayoubi, A.; Karsa, M.; Mayoh, C.; Henderson, M.J. Potent antileukemic activity of curaxin CBL0137 against MLL-rearranged leukemia. Int. J. Cancer 2020, 146, 1902–1916.
9. Burkhart, C.; Fleyshman, D.; Kohrn, R.; Commane, M.; Garrigan, J.; Kurbatov, V.; Gurova, K.V. Curaxin CBL0137 eradicates drug resistant cancer stem cells and potentiates efficacy of gemcitabine in preclinical models of pancreatic cancer. Oncotarget 2014, 5, 11038–11053.
10. Available online: (accessed on 29 April 2021).
11. Safina, A.; Cheney, P.; Pal, M.; Brodsky, L.; Ivanov, A.; Kirsanov, K.; Lesovaya, E.; Naberezhnov, D.; Nesher, E.; Koman, I.; et al. FACT is a sensor of DNA torsional stress in eukaryotic cells. Nucleic Acids Res. 2017, 45, 1925–1945.
12. Nesher, E.; Safina, A.; Aljahdali, I.; Portwood, S.; Wang, E.S.; Koman, I.; Wang, J.; Gurova, K.V. Role of Chromatin Damage and Chromatin Trapping of FACT in Mediating the Anticancer Cytotoxicity of DNA-Binding Small-Molecule Drugs. Cancer Res. 2018, 78, 1431–1443.
13. Leonova, K.; Safina, A.; Nesher, E.; Sandlesh, P.; Pratt, R.; Burkhart, C.; Lipchick, B.; Gitlin, I.; Frangou, C.; Koman, I.; et al. TRAIN (Transcription of Repeats Activates INterferon) in response to chromatin destabilization induced by small molecules in mammalian cells. eLife 2018, 7, e30842.
14. Kantidze, O.L.; Luzhin, A.V.; Nizovtseva, E.V.; Safina, A.; Valieva, M.E.; Golov, A.K.; Velichko, A.K.; Lyubitelev, A.V.; Feofanov, A.V.; Gurova, K.V.; et al. The anti-cancer drugs curaxins target spatial genome organization. Nature Commun. 2019, 10, 1441–1452.
15. Lu, K.; Liu, C.; Liu, Y.; Luo, A.; Chen, J.; Lei, Z.; Kong, J.; Xiao, X.; Zhang, S.; Wang, Y.-Z.; et al. Curaxin-Induced DNA Topology Alterations Trigger the Distinct Binding Response of CTCF and FACT at the Single-Molecule Level. Biochemistry 2021, 60, 494–499.
16. Kim, M.; Neznanov, N.; Wilfong, C.D.; Fleyshman, D.I.; Purmal, A.A.; Haderski, G.; Stanhope-Baker, P.; Burkhart, C.A.; Gurova, K.V.; Gudkov, A.V.; et al. Preclinical Validation of a Single-Treatment Infusion Modality That Can Eradicate Extremity Melanomas. Cancer Res. 2016, 76, 6620–6630.
17. Sergeev, A.; Vorobyova, A.; Yakubovskaya, M.; Kirsanova, O.; Gromova, E. Novel anticancer drug curaxin CBL0137 impairs DNA methylation by eukaryotic DNA methyltransferase Dnmt3a. Bioorg. Med. Chem. Lett. 2020, 30, 127296–127300.
18. Wang, W.; Hu, S.; Gu, Y.; Yan, Y.; Stovall, D.B.; Li, D.; Sui, G. Human MYC G-quadruplex: From discovery to a cancer therapeutic target. BBA Rev. Cancer 2020, 1874, 188410.
19. Jara-Espejo, M.; Line, S.R. DNA G-quadruplex stability, position and chromatin accessibility are associated with CpG island methylation. FEBS J. 2020, 287, 483–495.
20. Varizhuk, A.; Isaakova, E.I.; Pozmogova, G. DNA G-Quadruplexes (G4s) Modulate Epigenetic (Re) Programming and Chromatin Remodeling. BioEssays 2019, 41, 1900091.
21. Siddiqui-Jain, A.; Grand, C.L.; Bearss, D.J.; Hurley, L.H. Direct evidence for a G-quadruplex in a promoter region and its targeting with a small molecule to repress c-MYC transcription. Proc. Natl. Acad. Sci. USA 2002, 99, 11593–11598.
22. Agrawal, P.; Lin, C.; Mathad, R.I.; Carver, M.; Yang, D. The Major G-Quadruplex Formed in the Human BCL-2 Proximal Promoter Adopts a Parallel Structure with a 13-nt Loop in K+ Solution. J. Am. Chem. Soc. 2014, 136, 1750–1753.
23. Musso, L.; Mazzini, S.; Rossini, A.; Castagnoli, L.; Scaglioni, L.; Artali, R.; Di Nicola, M.; Zunino, F.; Dallavalle, S. c-MYC G-quadruplex binding by the RNA polymerase I inhibitor BMH-21 and analogues revealed by a combined NMR and biochemical approach. BBA Gen. Subj. 2018, 1862, 615–629.
24. Carvalho, J.; Mergny, J.L.; Salgado, G.F.; Queiroz, J.A.; Cruz, C. G-quadruplex, Friend or Foe: The Role of the G-quartet in Anticancer Strategies. Trends. Mol. Med. 2020, 26, 848–861.